J. Fluid Mech. (2007), *vol.* 571, *pp.* 97–118.
doi:10.1017/S0022112006003223 Printed in the United Kingdom

Bluff bodies in deep turbulent boundary layers: Reynolds-number issues

By HEE CHANG LIM[1], IAN P. CASTRO[1]† AND ROGER P. HOXEY[2]

[1]School of Engineering Sciences, University of Southampton, Highfield, Southampton, SO17 1BJ, UK
[2]Department of Civil Engineering, University of Birmingham, Edgbaston, Birmingham B15 2TT, UK

(Received 7 February 2006 and in revised form 21 June 2006)

It is generally assumed that flows around wall-mounted sharp-edged bluff bodies submerged in thick turbulent boundary layers are essentially independent of the Reynolds number *Re*, provided that this exceeds some (2–3) $\times 10^4$. (*Re* is based on the body height and upstream velocity at that height.) This is a particularization of the general principle of Reynolds-number similarity and it has important implications, most notably that it allows model scale testing in wind tunnels of, for example, atmospheric flows around buildings. A significant part of the literature on wind engineering thus describes work which implicitly rests on the validity of this assumption. This paper presents new wind-tunnel data obtained in the 'classical' case of thick fully turbulent boundary-layer flow over a surface-mounted cube, covering an *Re* range of well over an order of magnitude (that is, a factor of 22). The results are also compared with new field data, providing a further order of magnitude increase in *Re*. It is demonstrated that if on the one hand the flow around the obstacle does not contain strong concentrated-vortex motions (like the delta-wing-type motions present for a cube oriented at 45° to the oncoming flow), *Re* effects only appear on fluctuating quantities such as the r.m.s. fluctuating surface pressures. If, on the other hand, the flow is characterized by the presence of such vortex motions, *Re* effects are significant even on mean-flow quantities such as the mean surface pressures or the mean velocities near the surfaces. It is thus concluded that although, in certain circumstances and for some quantities, the Reynolds-number-independency assumption is valid, there are other important quantities and circumstances for which it is not.

1. Introduction

Over the last 30 years or so there have been increasingly numerous comparisons between full-scale (field) data and wind-tunnel data on both the flow around and the surface pressures on buildings of all kinds. The wind-tunnel experiments of Castro & Robins (1977) (hereafter denoted by CR) on surface-mounted cubes were some of the first to demonstrate the crucial importance of modelling appropriately the details of the upstream boundary layer. For smooth upstream flow conditions – i.e. when the thickness of the approaching boundary layer was very much smaller than the cube height – *Re* effects were found, not surprisingly. In contrast, for cases where the boundary-layer thickness was much larger than the cube, so that the flow 'seen' by the cube was fully turbulent (and highly sheared), no *Re* effects were reported for $Re > 4000$. It must be noted, however, that this conclusion rested on somewhat limited

† Author to whom correspondence should be addressed: i.castro@soton.ac.uk

data and was not a result of an extensive study of possible *Re* effects; the major thrust of that early work was to highlight the importance of ensuring appropriate simulation of the atmospheric boundary layer. But there has since been some wind-tunnel evidence, albeit over rather restricted Reynolds-number ranges, that $Re > (2–3) \times 10^4$ is sufficiently high to ensure negligible *Re* effects (e.g. Cherry, Hillier & Latour 1984; Djilali & Gartshore 1991) and such an assumption has formed the basis of most model scale testing for almost half a century. However, *Re* independency has more recently been questioned, not only conceptually (by, significantly, one of the 'fathers' of wind engineering; see Davenport 1999) but also as a result of relatively new data obtained in the field (e.g. Hoxey *et al.* 1998; although, again, this data was obtained over a very restricted *Re* range).

It is not difficult to imagine why the Reynolds number could remain an important parameter even when $Re > (2–3) \times 10^4$. This is particularly true for those flows in which the shear layers arising from separation of the boundary layers at the salient edges of the body roll up rapidly to form concentrated relatively steady vortical regions. The most obvious example is for bodies at an angle to the approach flow, on which strong conical vortices appear, similar to those above delta wings. Such vortices are often less affected (than the Kelvin–Helmholtz-type vortices arising in other kinds of separated shear layers) by changes in upstream flow characteristics, partly no doubt because they are usually a much more persistent feature of the generally unsteady flow; see e.g. Kawai (2002) for a discussion of their dynamics. Their viscous cores have a relative size and influence that must be dependent on a Reynolds number based on the thickness of the rolled-up vortex sheet, so this dependency may persist well beyond $Re > (2–3) \times 10^4$, since the latter *Re* is based on a typical body dimension, h. Practically important flow characteristics, like the peak-suction surface pressures which usually occur near salient edges and beneath these conical vortices, would then also be dependent on *Re* over a wider range than in cases where such strong vortex motions are less prevalent.

In comparisons between model tests and full-scale tests, assessing *Re* effects is complicated by the known effects of changes in upstream turbulence intensity and scale on bluff-body flows and also by the inevitable mismatch in spectral-energy content in the upstream flow between atmospheric boundary layers and wind-tunnel simulations of them. There is a significant literature on both these topics. In the case of the former, one might note as an example the relatively recent work of Saathoff & Melbourne (1997) (and many references therein). Recognizing that one of the flow features most likely to be dependent on upstream-turbulence characteristics is the fluctuating pressure near the leading edges of the body, they conducted experiments on a generic body, a two-dimensional blunt flat plate (thickness h). Measurements with a variety of upstream conditions showed conclusively that increases in upstream turbulence intensity σ_u/U and/or integral length scale L_x/h increased the magnitude of the pressure fluctuations measured at a point on the surface very near the leading edge and underneath the separated shear layer. The mean flow was likewise significantly affected; the length of the separated bubble, for example, noticeably decreased with increasing σ_u/U. The effects can be explained on the basis of the dynamics of the separating shear layer and its vorticity field and are consistent with the findings of Hillier & Cherry (1981) and, incidentally, with those of CR for a cube. Such behaviour provides some explanation for flow differences commonly found between model and full-scale situations which, although ostensibly similar, may not be sufficiently similar in terms of the upstream turbulence field. Any differences caused by the large *Re* discrepancy can be masked by those due to differences in the background turbulence.

The second issue noted above, that of spectral mismatch, is also well known. In wind-tunnel modelling of single buildings in atmospheric boundary layers, for example, it is common and indeed often necessary to use quite large scales (e.g. 1 : 100); this usually means that the largest turbulence scales in the simulated flow are much smaller than the full-scale equivalents. The question arises as to which part of the turbulence energy spectrum should be matched most closely. It has become clear that merely matching the upstream longitudinal integral scale and the turbulence intensity (at the body height, say) does not necessarily produce good agreement between the full-scale and model-scale data. Melbourne (1980) argued that, in fact, matching the small-scale turbulence levels is much more important in determining the peak (negative) pressures occurring near salient edges of the body, and he suggested a 'small-scale spectral-density parameter' S_m, defined (for the present case) by $S_m = f S_u(f)/U_h^2$ evaluated at $f = 10U_h/h$, where $S_u(f)$ is the usual longitudinal spectral energy density at frequency f and $z = h$ and U_h is the mean velocity at $z = h$. The essential reasoning is that $f = 10U_h/h$ typifies the scales in the surrounding turbulence which are most likely to affect the dynamics of the separated shear layers, whose thicknesses are, initially at least, much smaller than the body dimension, and typically $O(0.1h)$. There is some evidence that this approach produces much closer agreement between model-scale and full-scale data (see Tieleman 2003, for example). Nonetheless, the effect of the relatively much larger integral scales at full scale, particularly those characterizing the cross-stream fluctuations, cannot easily be reduced. The relatively large cross-stream integral scale is associated with relatively larger cross-stream excursions in the unsteady wind direction and this has unavoidable affects, even on the mean flow around the body let alone on fluctuating quantities like the r.m.s. pressure coefficients.

The major difficulties in assessing the overall Reynolds-number effects are therefore twofold. First, at model-scale, one must be sure that in varying *Re*, which is usually done in an experiment by varying the flow speed, the upstream turbulence characteristics covering as wide a spectral range as possible do not change significantly. Second, in the context of comparing model-scale and full-scale data, one must take account of the almost inevitable differences caused by the differences in the boundary layers' largest-scale motions, even if simulations have been assiduously arranged to ensure similarity in, say, Melbourne's parameter, S_m. In wind-tunnel simulations of typical neutrally stable atmospheric boundary layers there is limited scope to vary *Re* by more than, typically, a factor of about 3. Changes in free-stream velocity greater than this factor would often lead to significant changes in the boundary-layer characteristics (because of, for example, transitional surface roughness effects at the lower velocities) and changes in body size would require a completely new set of boundary-layer-simulation hardware. It should be emphasized that flow changes with *Re* will be most rapid at the lower end of the *Re* range, so if they are not evident there they are unlikely to exist at higher *Re*.

In this paper we describe a carefully designed set of experiments on boundary-layer flow over a surface-mounted cube, undertaken in two wind tunnels, of sufficiently different sizes to allow variation in *Re* by a factor of 22 to be achieved with little change in upstream-boundary-layer characteristics. Data is also presented from corresponding field measurements, yielding a further order-of-magnitude change in *Re*. The wind-tunnel flows were designed to be similar to the (rural) atmospheric boundary layer approaching the 6 m cube in the field experiments. Here, emphasis is placed largely on the extent to which the flows were affected by *Re* and attention is concentrated on the two cases defined by cube orientations of zero and 45° to the approach flow. The latter case typifies flows in which strong, relatively steady,

concentrated vortex regions exist over the obstacle; the former is, in that respect, very different. One could thus view these two cases as examples of two extremes in the whole range of possible flow types, for a whole range of possible shapes of sharp-edged bodies. The following section outlines the experimental techniques, § 3 summarizes the flow characteristics in both wind-tunnel and field boundary layers approaching the cubes and § 4 presents and discusses the major results; § 5 gives the major conclusions.

2. Experimental techniques

2.1. *Laboratory methods*

Experiments were conducted in the large closed-circuit 'R. J. Mitchell' wind tunnel, whose working section dimensions are 3.4 m × 2.5 m × 8 m long, and a much smaller 0.9 m × 0.6 m × 4.5 m open-circuit tunnel, both within the School of Engineering Sciences at the University of Southampton. Thick boundary layers were generated using a technique often employed by wind-engineering practitioners, first devised by Cook (1973, 1978). Toothed barriers spanning the floor of the working section near its entry, followed by a square section, biplanar mesh across the entire working section and an appropriate rough surface thereafter can together be designed to yield mean-velocity profiles which are closely logarithmic over a significant portion of the working-section height, with turbulence stresses and spectra similar to those found in atmospheric neutrally stable boundary layers. There are other ways of simulating atmospheric boundary layers (see Hunt & Fernholz 1975, for an old, but still appropriate, review); this particular method has the advantage of maximizing the depth of the logarithmic region but the disadvantage of not simulating the largest-scale eddies in the upper part of the atmospheric boundary layer. For the present purposes, since it was intended to make comparisons with full-scale data over a cube merely 6 m in height – less than one-tenth of the height of the logarithmic region – maximizing the depth of this region was deemed most important. It is crucial to design the barrier wall and mixing-grid geometries in tandem with the intended roughness, since any mismatch will yield unacceptably long fetches before reasonably well-developed flows are attained. In the present cases, commercially available expanded aluminium mesh was used to provide the surface roughness; the mesh for the smaller tunnel had a total height of 3 mm and that for the larger was roughly three times the size in all salient respects. These gave roughness lengths z_0 of 0.09 and 0.35 mm, respectively, where z_0 is defined in the usual way via the mean-velocity log law expressed as

$$\frac{U}{u_*} = \frac{1}{\kappa} \ln \frac{z-d}{z_0}. \tag{2.1}$$

Here u_* and d are the friction velocity ($\sqrt{\tau_{wall}/\rho}$) and the zero-plane displacement, respectively. Since (2.1) contains three unknowns (u_*, d and z_0), use only of a measured mean-velocity profile (i.e. U versus z) to obtain all three parameters is somewhat ill-conditioned (although it is the approach which frequently has to be used by meteorologists!). It is generally accepted that a significantly better alternative is to measure the friction velocity independently, by extrapolating turbulence-stress measurements to the wall, and then to fit the separate mean-velocity data to (2.1) to ensure the correct u_* by adjusting d appropriately. This yields a z_0 estimate. In the present work, boundary layers grown naturally over the mesh surfaces (i.e. without an upstream barrier and mixing grid) were examined to determine z_0 and d, using the approach outlined above. As will be shown in due course, the resulting values

provided satisfactorily consistent data in the simulated flows. For the smaller tunnel, the barrier wall had a height of 62 mm, with triangular cut-outs at the top, of pitch 50 mm and depth 50 mm, and the mixing grid consisted of a biplanar grid of 9 mm bars at a pitch of 60 mm. The barrier and mixing grid used in the larger tunnel were approximately a factor of 3 larger than those used in the smaller tunnel, with the intention that the boundary-layer characteristics would (at appropriate fetches) be very similar in the two tunnels.

Smooth-surface cubes of height h equal to 240 mm or 80 mm were used in the larger and smaller tunnels, respectively, and were fitted with 0.8 mm i.d. pressure taps at numerous salient points on the top surface and the front and rear faces. Standard tube connections to a (Furness FC-012) micromanometer allowed the measurement of mean surface pressures. The fluctuating pressures were obtained using both piezoresistive sensors (Endevco 8507C-2) and omnidirectional condensor-type microphones (Panasonic WM-60A). The former had a diameter of 1.27 mm and a frequency response which was flat from d.c. to around 15 kHz, whereas the latter were of diameter 6 mm and so were each mounted in a small cavity beneath a 0.5 mm pinhole in the surface, yielding a response which was flat between 20 Hz and 20 kHz.

Mean-velocity and turbulence-stress data within the boundary layers at the (subsequent) cube locations and around the cubes themselves were obtained using appropriate combinations of hot-wire anemometry (HWA), laser-Doppler anemometry (LDA) and particle-image velocimetry (PIV) systems. For HWA, errors caused by inadequate yaw response were minimized by using crossed-wire probes with $\pm 60^\circ$ wires (rather than the more standard $\pm 45^\circ$ wires, see Perry, Lim & Henbest 1987) and employing the effective-cosine-law method to calibrate for yaw sensitivities. The probes had wires of about 1 mm in length and were driven by Newcastle (NSW) CTA bridges, with outputs filtered to avoid aliasing and massaged by appropriate gain and offset to allow the best use of the analogue–digital converters (IOTech ADT488). Calibrations were performed against a standard pitot-static tube using the same micromanometer as was used for the (static) pressure measurements, and all analogue signals were digitized and passed to a (Macintosh) desk-top computer. Specialized software ('Virtual instruments', written in National Instruments' LabVIEW) allowed on-line calibration and measurement of all necessary quantities. The probes were supported on traverse systems driven by the same computer. Sampling rates were typically between 2 kHz and 10 kHz, depending on the quantities being measured, with sample times of 60–120 s.

For LDA, a two-component fibre-optic Dantec system was used, with burst-spectrum analysers (BSAs) to process the Doppler bursts. Since turbulence intensities close to the surface and near to the cube were often greatly in excess of 25 %, interval time weighting was used in obtaining the mean and fluctuating velocities. The same software package as used for HWA and pressure measurements was employed. (This actually allows simultaneous HWA and LDA measurements, but that facility was not used in the present work). In the small-tunnel experiments, the probe was located outside the working section, with the beams transmitted through the perspex side walls. Since the lens focal length was 300 mm, the measurements were made in a plane a little away from the tunnel centreline but, given the high degree of spanwise uniformity in the flows, this was quite acceptable. In the large tunnel, the probe had to be located on a suitable traverse system inside the working section and this was always arranged so as to minimize the possible influence of blockage. In both tunnels the beams were oriented so as to measure the axial and vertical velocity components.

The work presented here was undertaken in the context of a much larger study, in which PIV has been used extensively (to identify flow structures, etc.). Here we will present only a very small subset of the PIV data, as a means of clarifying some resolution issues for the field ultrasonics (see § 2.2 below). Both a Dantec system and a TSI system were used. Each employed the same New Wave Gemini 120 mJ Nd:Yag dual-fire laser to illuminate the field, usually in vertical planes oriented at various angles to the axial direction. In the former case, a 80C60 HiSense camera (1280×1024 pixels) was used, with final interrogation areas of typically around 1.2 mm^2, whereas in the latter case a camera (2048×2048 pixels) with final interrogation areas of around 0.6 mm^2 was employed, to give greater spatial resolution where necessary. In both cases, the use of recursive algorithms designed to allow the shifting of successive interrogation areas by an amount depending on the local velocity (Hart 2000) was necessary to minimize errors. Typically, final interrogation areas of 16×16 pixels with a 50 % overlap were used. The resulting vectors were validated using a simple peak-height scheme and the number of rejected vectors was always below 5 % and usually much lower. Typically, 1000 image pairs were obtained in every case; this was a compromise between minimizing the statistical errors arising from a finite sample size and maintaining a reasonable total sampling time. With sampling rates of around 2 Hz, the latter was typically around 500 s. Seeding for both LDA and PIV measurements was provided either by a hydrosonic seeder or a standard smoke machine. Both yielded particles of appropriate size, whose image sizes were 2–4 pixels in the PIV case.

2.2. *Field methods*

Field measurements were carried out on a 6 m smooth-surfaced cube mounted on a turntable in a level open field site at Silsoe Research Institute. The approach fetch for all the data presented herein was low grass extending at least 600 m upstream and both previous and our current data indicated that under neutrally stable conditions the mean-velocity profile is well fitted by (2.1). The present data gave a z_0 value around 8 mm, obtained using the technique discussed in § 2.1 from data given by four ultrasonic anemometers mounted on the reference mast (see below). This gives a Jensen number, $Je = h/z_0$, of 750, within the range 690 to 890; these were the values for the large- and small-tunnel tests, respectively. The cube was instrumented with 9 mm internal-diameter surface-static-pressure tappings, allowing up to 16 simultaneous pressures to be obtained. Upstream wind-velocity components were derived from a three-dimensional ultrasonic anemometer at the cube height, mounted on a mast $3.4h$ upstream of the front face of the cube and $1.04h$ beyond a side face – sufficiently removed from the cube for the data not to be influenced by it and for the mast not to influence the flow over the cube. The pressure signals were transmitted to solid-state transducers with a range of ± 0.6 kPa, using 6 mm internal diameter plastic tubing up to 5 m in length, arranged to give an overall frequency response flat to around 8 Hz. Transducer drift was invariably small but was nonetheless corrected by means of a computer-controlled sequence which applied a zero pressure, followed by the total pressure from a pitot-static tube mounted upstream, to all the transducers at the beginning and end of every 30 minute record. Typically, pressures were sampled at 25 Hz. For all the data presented here, only the central 20 minutes of the 30 minute records have been used.

It was important to select only those records which corresponded to the required wind orientation with respect to the cube and for which the data suggested genuinely neutral conditions. For the former, the upstream ultrasonic records were scrutinized

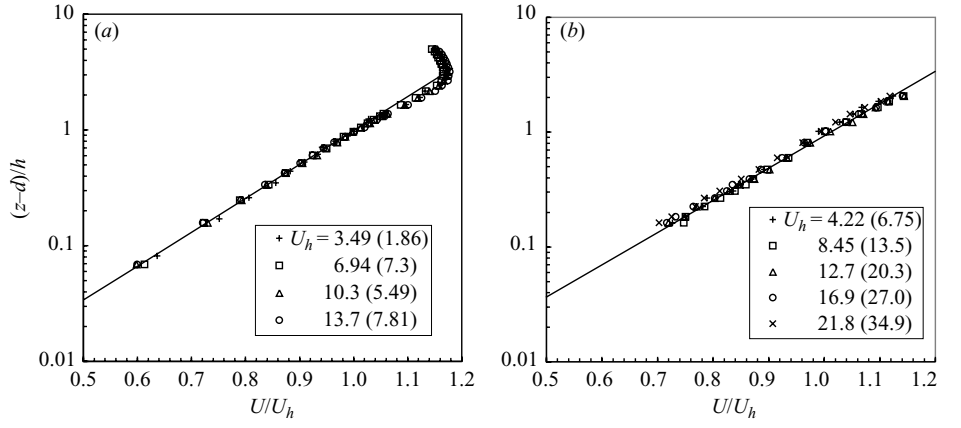

FIGURE 1. Mean-velocity profiles: (*a*) small tunnel; (*b*) large tunnel. Figures for the velocity at cube height, U_h, are in $\mathrm{m\,s^{-1}}$ with $Re \times 10^{-4}$ (based on the appropriate h) in parentheses. The solid lines give the log law (2.1).

to ensure that they did not contain sudden shifts in wind direction other than those attributable to genuine turbulence and also to deduce the mean wind direction. Only those records indicating directions (averaged over the 20 minute record length) which were within $\pm 2^\circ$ of that required were selected. For the latter, the ultrasonic outputs included sound-speed data allowing deduction of the temperature. (Note that, even for fully saturated air, changes in sound speed arising from specific humidity changes can be shown to be entirely negligible compared with those arising from direct temperature variations.) The implied temperature data can be used to deduce $-\overline{w\theta}$, the Monin–Obukhov length scale L_{MO} and the obstacle Froude number, $Fr = U/Nh$, where N is the Brunt–Vaisaila frequency. In all cases Fr was large enough – $O(10)$ at least – to suggest that buoyancy effects on the flow over the cube would be totally insignificant (see Snyder 1994 for a discussion of this point). However, there were records for which the values of h/L_{MO} indicated that the upstream profile over the cube height might have been slightly stable or even unstable. Such records are not included in the present analysis.

Simultaneous measurements of velocities over the cube were also made using a further four (Solent WindMaster) ultrasonic anemometers. These were located 0.06 m ($0.01h$) above the top surface and, usually, along an axial line 500 mm ($0.083h$) away from the centreline, so as to avoid disturbance at the centreline static pressure holes. Both these and the upstream sonic provided samples at 25 Hz over the identical 30 minute periods used to obtain the pressure records. Reference static pressure was provided in all cases by the heavily damped output of an upstream surface-static tapping, set flush into the ground some $4h$ upstream of the cube. Calibration against mast-mounted instruments showed that this provided an accurate and appropriate reference.

3. The upstream boundary layers

3.1. *Wind-tunnel flows*

All mean- and fluctuating-velocity data were normalized using the mean velocity at the cube height, U_h. The (LDA) mean-velocity profiles obtained over a range of wind speeds in each tunnel are shown in figure 1. In each case the profiles were obtained

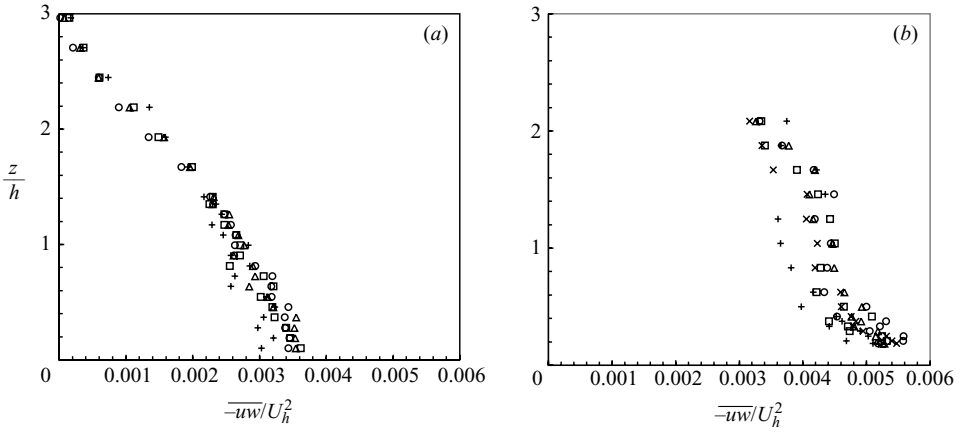

FIGURE 2. Reynolds-shear-stress profiles: (*a*) small tunnel; (*b*) large tunnel. Symbols as in figure 1.

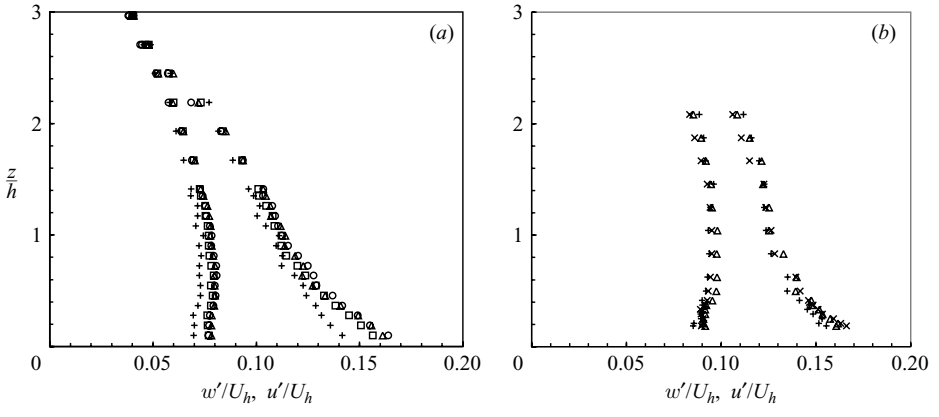

FIGURE 3. Turbulence intensity profiles: (*a*) small tunnel; (*b*) large tunnel. Symbols as in figure 1.

at the eventual cube location, 3.5 m and 7 m downstream from the barrier wall in the small and large tunnels, respectively. Notice in particular that the velocity ranges imply Reynolds-number ($Re = U_h h/\nu$) variations of $1.86 \times 10^4 \leqslant Re \leqslant 7.31 \times 10^4$ and $6.75 \times 10^4 \leqslant Re \leqslant 3.49 \times 10^5$ in the small and large tunnel, figures 1(*a*) and 1(*b*) respectively, and that in neither case is there any significant profile change with *Re*. The two *Re* ranges overlap and, together with additional HWA data from the large tunnel (not shown for clarity), yield a factor 22 variation in *Re*. The fits to (2.1) extend at least to $z = 2h$ in both cases, so the cubes are submerged well within the log-law region. Figures 2 and 3 show the corresponding profiles for the Reynolds stress $-\overline{uw}$ and the intensities u' and w'. The data do not extend beyond $z/h = 2$ in the large tunnel but are quite adequate for demonstrating the Reynolds-number independence of the profiles. Note that the intensities and stresses are a little higher in the large tunnel. This is almost certainly a result of a rather smaller equivalent fetch, $29h$ compared with $44h$ in the smaller tunnel. The flow is probably still developing at this axial location; this would account also for the slightly different shape of the stress

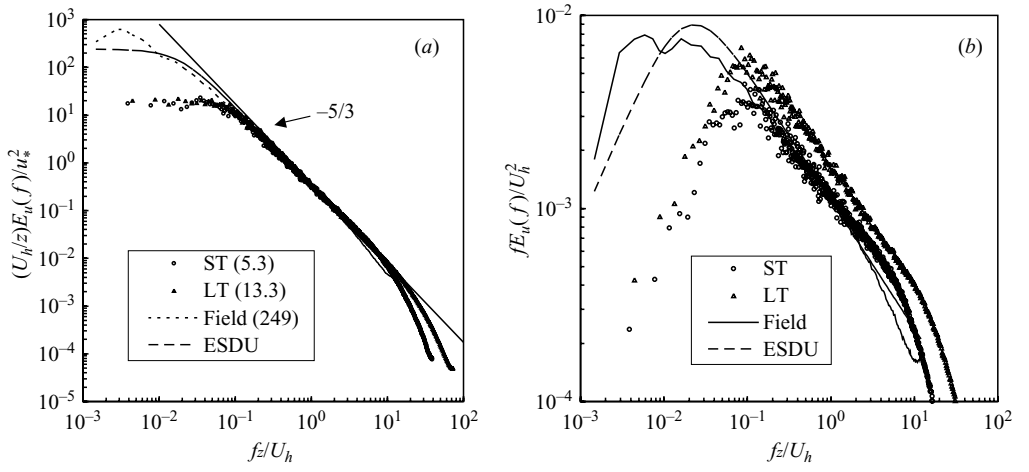

FIGURE 4. Spectra of the axial turbulence component at $z = h$; (*a*) normalised by $\overline{u^2}$, with $Re \times 10^{-4}$ values given in brackets; (*b*) normalised using U_h^2. ST, small tunnel; LT, large tunnel.

profiles in figure 2(*b*) compared with those from the smaller tunnel in figure 2(*a*). However, any remaining axial-flow development at the cube location in the large tunnel is most unlikely to be important, and the differences in stress levels between the two tunnels are not significant compared with those which might be expected to yield noticeable changes in the flow around the cube. At the cube height, for example, the longitudinal turbulence intensities (figure 3) are 11.2 % and 13.2 % in the small and large tunnels, respectively. These may be compared with the field value of around 18 %; possible effects of this rather larger difference are discussed in due course.

Figure 4 presents longitudinal-velocity spectra, $E_u(f)$, obtained at $z = h$. In figure 4(*a*) the spectra are plotted in the form in which collapse in the inertial subrange may be expected, whereas in figure 4(*b*) they are normalized in a common wind-engineering form, using parameters independent of the turbulence; this is more appropriate for revealing differences in the small-scale energy levels. The results are discussed in detail, in comparison with standard spectra for the atmospheric surface layer and with the field spectra, in the following section.

3.2. *Field data*

Mean-velocity and turbulence statistics at the Silsoe site have been measured a number of times over recent years (e.g. Richards, Hoxey & Short 2000; Richards & Hoxey 2004) and further data has been accumulated as part of the current project. It has become clear that under neutral conditions the flow characteristics depend critically on the local wind direction. As an example, figure 5(*b*) shows measurements at $z = h$ of the longitudinal turbulence, i.e. the r.m.s. intensity of the velocity component in the mean wind direction, measured over each of 120 (20 minute) records, as a function of the wind direction ϕ; $\phi = 0$ corresponds to the direction of the inward normal to the front face of the cube – actually a geographical direction of 58° from true North, see figure 5(*a*). These records were obtained in the period January–March 2004. The Reynolds shear stress is also shown. The mean wind direction for each record was taken as that implied by V/U, where V and U are the orthogonal velocities in the horizontal plane averaged over that record. Only records which did not contain sudden changes in overall wind direction, as indicated for example by noticeable

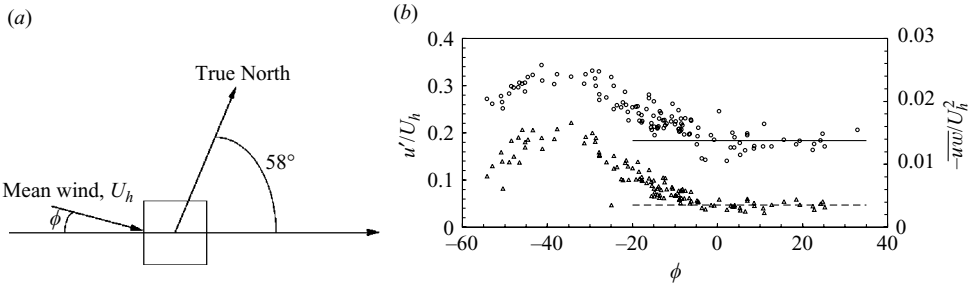

FIGURE 5. (*a*) Cube orientation and definition of ϕ. (*b*) Turbulence intensity (left-hand scale, circles) and Reynolds shear stress (right-hand scale, triangles) at $z = h$, as a function of the mean wind (U_h) direction. The solid line is the u'/U_h value averaged over $-5^\circ \leqslant \phi \leqslant +5^\circ$ and the dashed line is the corresponding average Reynolds shear stress.

bimodality in the probability densities of v' or $\arctan(v'/u')$, are included in the figure and in the subsequent analysis. (Here u' and v' are the fluctuating velocities, rather than the r.m.s. values). It is clear that for wind directions between about -5° and $+35^\circ$ both the longitudinal intensity and the Reynolds shear stress can be assumed to be roughly constant, at around 0.182 and 0.0035, respectively, whereas for $\phi < -10^\circ$ there is a gradual increase in turbulence levels. This corresponds to a significant change in upstream topography for the latter wind directions; it becomes much rougher because of the presence of more trees, shrubs and low buildings.

The vertical and lateral turbulence intensities w'/U_h, v'/U_h averaged over the same range of wind directions were around 0.082 and 0.151, respectively. Although the former is close to the wind-tunnel values (see figure 3), v' is rather higher, as is u'. However, the field data, including ratios such as u'/u_* and v'/u', are within the ranges expected for a rural-type (neutrally stable) boundary layer; see, for example, ESDU (1985). The differences in the horizontal intensities between field and wind-tunnel boundary layers are typical, and the possible effects on the cube flows will be discussed in due course; they are largely a result of the largest-scale motions, which cannot be reproduced at wind-tunnel scales. Note, incidentally, the significant degree of scatter in the data in figure 5, even within the wind-angle range deemed to yield approximately constant characteristics. The scatter is typical of field data and is much larger than occurs in laboratory data. It cannot be accounted for by the slight non-neutrality of the boundary layer in a few cases included in the figure and is generally thought to be the result of the inherent non-stationarity of the flow.

The longitudinal spectra, averaged for all the data obtained in the range $-5^\circ < \phi < +25^\circ$ are included in figure 4 and illustrate the fact that it is not possible to match both the large-scale and the small-scale turbulence. Figure 4(*a*) suggests that if the integral length scale were deduced from the $E(0)$ asymptote (and normalized by h) the field value would be very much larger than the values in the two tunnel boundary layers. One can write $L_x/h = (U/hu_*^2)(u_*^2/\overline{u^2})(E(0)/4)$ so that whilst this yields around 1.4 for the tunnel boundary layers it gives a value somewhere in the range 10–15 for the Silsoe site (depending on the precise value chosen for $E(0)$). But it is well known that this method of estimating the integral scale is, for the field data, very problematic; equivalently, deducing L_x from autocorrelations is not possible for field data since the inherent non-stationarity gives autocorrelations which for the longitudinal and transverse components do not have zero crossings. It is better to use one or other of the usual spectral shapes typical of near-surface data. Kaimal

	u'/U_h	v'/U_h	w'/U_h	$-\overline{uw}/U_h^2$	h/z_0	L_x/h	S_m	λ/h
$3' \times 2'$ tunnel	0.114	0.089	0.078	0.0027	890	1.38	0.000236	0.130
$11' \times 8'$ tunnel	0.136	—	0.096	0.0044	690	1.46	0.000406	0.075
Field	0.182	0.151	0.082	0.0035	750	6.4–6.9	0.000161	0.027

TABLE 1. Salient parameter values at $z = h$. S_m refers to the parameter Melbourne (1980), $fS_u(f)/U_h^2$ at $f = 10U_h/h$, which, along with λ, is calculated from the spectra in figure 4.

et al. (1978), for example, suggested a spectral shape for the near-surface neutral atmospheric boundary layer given by

$$\frac{fE_u(f)}{u_*^2} = \frac{102n}{(1+33n^2)^{5/6}}, \tag{3.1}$$

where $n = fz/U$ and U is the mean velocity at the height z where $E_u(f)$ is measured. In the inertial region this becomes $fE_u(f) = An^{-2/3}$ with $A = 0.3$. Now the classical Kolmogorov spectrum can be written as

$$fE_u(f) = C\epsilon^{2/3}(2\pi f/U)^{-2/3}. \tag{3.2}$$

Assuming that in the surface layer the flow is in equilibrium so that, using the log law, ϵ can be replaced by $u_*^3/(\kappa z)$, these two expressions are equivalent provided that $C = 0.55$. Although it is just within the range suggested in the literature, this is a rather larger value of C than the current consensus of 0.49 (see, for example, Pope 2000). Accepting the latter value would, for equivalence, require $A = 0.265$ in the Kaimal spectrum, which is the value used by Richards *et al.* (2000) in their analysis of surface-layer spectra. A common alternative for the spectral shape is that provided by ESDU (1985):

$$\frac{fE_u(f)}{\overline{u'^2}} = \frac{4n'}{(1+70.8n'^2)^{5/6}}, \tag{3.3}$$

where $n' = fL_x/h$ and L_x is the longitudinal integral scale. This is equivalent to the Kaimal spectrum in the inertial subrange if L_x is related to the turbulence statistics via $L_x/h = 0.237(\overline{u'^2}/u_*^2)$; for the present field data, this suggests a value for L_x some 10 % larger than that given by fitting the measured data to the ESDU spectrum. The latter procedure yields $L_x = 38.2$ m, much lower than the value suggested by the $E(0)$ asymptote (60–90 m), as noted above, and is usually seen as the preferred way to estimate L_x from the atmospheric-boundary-layer data. Since the wind-tunnel flows are intended to be simulations of the field situation, all the spectral data, both in the field and in the wind tunnels, were fitted to the ESDU spectrum and the fits yielded the values of L_x/h given in table 1. For the wind-tunnel cases, these values are very consistent with those obtained from $E(0)$ but, nonetheless, all values could be viewed as estimates since their precision depends, of course, on the values taken for the constants A, κ, on whether these are forced to yield an appropriate fit to the Kolmogorov spectrum in the inertial subrange and on the extent to which Taylor's hypothesis (implicit in all the spectral relationships given above) is valid.

Note that the data in the inertial subrange appear to collapse quite well (figure 4*a*). However, this kind of plot can be misleading in this respect since the spectral density is normalized by a turbulence parameter (u_*^2 in this case). Figure 4(*b*) shows that although there are some differences in the spectral energy at the small scales, the variations are much smaller than the variations in L_x/h. In particular, Melbourne's

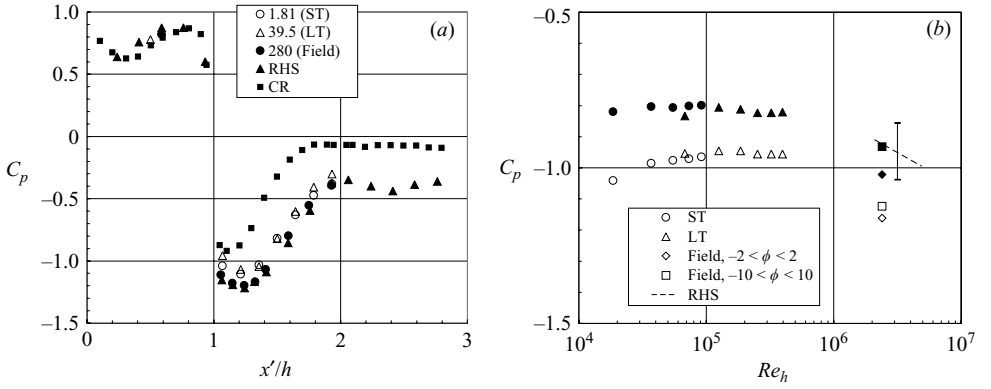

FIGURE 6. (*a*) Mean surface static pressure along the centreline of the cube. x' is measured around the three faces, with $x' = 0$ at the upstream base; $1.0 \leqslant x'/h \leqslant 2.0$ is thus the top surface. The legend gives the values of $Re \times 10^{-4}$ for each case, with the data source indicated: ST, small wind tunnel; LT, large wind tunnel; RHS, Richards *et al.* (2001); CR, Castro & Robins (1977). (*b*) The data at $x'/h = 1.069$ (open symbols) and near the central point, $x'/h = 1.5$ (solid symbols); the dashed line is the trend line from Richards *et al.* (2001), with the range of values indicated by the vertical bar.

small-scale turbulence parameter (Melbourne 1980) (see § 1) is within a factor 2.5 for the three cases. Possible effects of the inevitable mismatch in the large scales between tunnel and field on the measurements on and around the cube are discussed later. It is worth noting that the Reynolds number based on the Taylor microscale λ for the longitudinal velocities, $Re_\lambda = u'\lambda/\nu$, varies from 840 in the $0.9\,\mathrm{m} \times 0.6\,\mathrm{m}$ tunnel to 1350 in the $3.4\,\mathrm{m} \times 2.5\,\mathrm{m}$ tunnel to 13 000 in the field, for the spectra shown in figure 4. This is, as expected, a variation roughly proportional to $Re^{0.5}$ and is much larger than the variation in the Melbourne parameter. The ratio λ/h is 0.13, 0.075 and 0.027 in the three cases, respectively. Again, the implications are discussed later. Table 1 summarizes the values of the salient parameters for the two wind tunnels and the field situation. The values of the turbulence intensities and the Reynolds shear stress shown are averages in each of the wind-tunnel cases; the variations with Re are within $\pm 2\,\%$ for the mean velocity and $\pm 8\,\%$ for the second-order statistics – only marginally larger than the expected experimental uncertainties for those quantities.

4. Results and discussion

4.1. *Mean-flow data*

We consider first the surface pressure field on the cube. Figure 6(*a*) presents the variation of the mean static pressure C_p along the axial centreline of the cube, obtained in both wind tunnels and in the field for the normal case ($\phi = 0$). Only a selection of data is included, for clarity; the data at the lowest tunnel speed for the smaller tunnel and at the highest speed for the larger tunnel are shown. This provides around a factor of 22 in Re, the field data providing a further factor of 7. C_p is defined as $(p - p_r)/(0.5\rho U_h^2)$, where p_r is the mean static pressure in the upstream flow. For the wind-tunnel data, this was obtained in the free stream upstream of the cube; the variation vertically through the flow was negligible. In the field, the reference pressure was from the surface tapping (see § 2.2). Note that the Richards, Hoxey & Short (2001) data was originally presented as pressure coefficients normalized by the mean of the upstream dynamic pressure, i.e. using $\overline{(U + u')_h^2}$ rather than U_h^2 (here u'

is the fluctuating component of the longitudinal velocity). Using the latter rather than the former was found to yield C_p values typically some 7 % higher in magnitude, so their field data presented here has been factored appropriately. The profiles in figure 6(*a*) have the expected shape, in that the largest negative pressures occur just beyond separation and are followed by a substantial pressure recovery associated with the attachment process on the top surface, as shown frequently by previous studies. Note that the data agree well with the earlier field data of Richards *et al.* (2001) at the same site but are significantly different from the wind-tunnel data of CR. The latter are similar to those of Murakami & Mochida (1988) and, in agreement with CR's discussion, are undoubtedly a result of very much higher upstream turbulence levels, leading to much earlier attachment and pressure recovery on the top surface.

The immediate implication of the data in figure 6(*a*) is that there appears to be little Reynolds-number effect. This is emphasized in figure 6(*b*), which shows C_p at the centre of the top surface and at a location just beyond the leading edge as a function of *Re*, using all the data available from the present experiments. Note that several subsequent figures are arranged in a similar manner to figure 6, i.e. transect profiles are shown on the left and variations with *Re* are shown on the right, at one or more specific locations where one might expect the *Re* effects to be greatest. It is worth emphasizing again that such effects would normally be expected to be greatest (per decade of *Re*, say) at the lower Reynolds numbers. The fact that even the small-scale data in figure 6 show no variation over a factor of over 20 in *Re* would immediately suggest little likelihood of change with further increases in *Re*. Note, however, that at the location near the leading edge (open symbols) there is a hint of a small *Re* effect at the lower end of the *Re* range. One would eventually expect such an effect as the *Re* value falls, not only because of the reducing extent of the inertial subrange in the upstream spectrum (although Re_λ is always above about 500) but also because the boundary layer separating at the leading edge will be laminar, with the subsequent transition in the shear layer occurring nearer and nearer the separation point as *Re* rises. Once *Re* exceeds about 3×10^4, the changes are very small; this is consistent with conventional wisdom. Figure 6(*b*) shows that the field experiments clearly yield significantly lower C_p values. The data points shown were obtained by averaging the results from all the available 30 minute records for which the averaged wind direction was within $\pm 2^\circ$ or $\pm 10^\circ$ of the normal to the cube's front face. Increasing the allowable range of wind directions increases the resulting averaged C_p, but the differences indicated are within the scatter of all the data. Only three records satisfied the $\pm 2^\circ$ criterion, compared with 37 for the wider range. However, the *Re* value for these 37 varied by a factor of about 2.8.

In an attempt to assess whether this field data showed any trend with *Re*, and to increase the number of available data points, the central 20 minutes of each record was split into four five-minute records. The trends in the resulting C_p values plotted against *Re* suggested that C_p increases with *Re* (but with little statistical significance) whereas Richards *et al.* (2001), using somewhat larger data sets, found an exactly opposite trend. However, we believe that it remains more likely that the lower C_p values in the field are a result simply of the relatively larger turbulence energies at the lowest frequencies in the upstream flow (see § 3.1), as is frequently argued (e.g. CR), and that little variation with *Re* is discernible. (Note that there is no unequivocal way of separating these contributions from the larger-scale motions.) In any case, there is certainly no theoretical justification for a *Re* trend within the range of, say, $10^6 < Re < 10^7$ if one does not exist in the lower range of, say, $10^5 < Re < 10^6$.

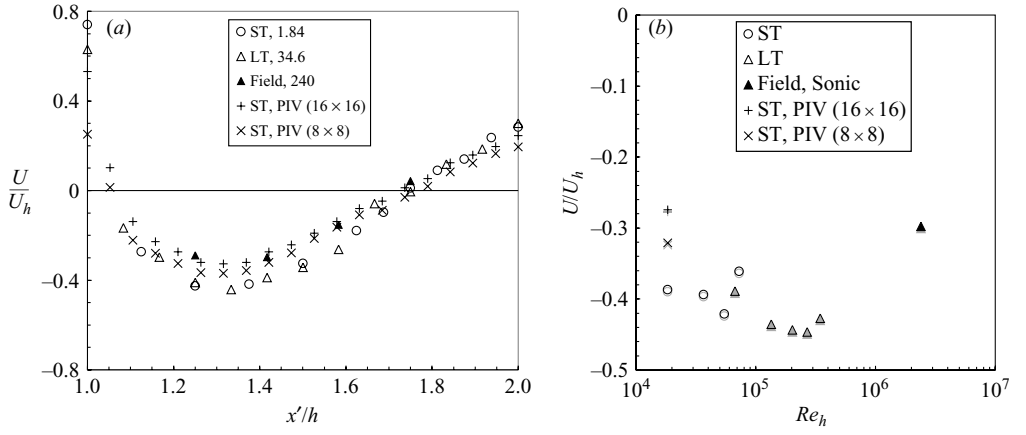

FIGURE 7. (*a*) The axial velocity along the line $y = 0$ parallel to the top surface of the cube and at $0.01h$ above it. The legend gives the values of $Re \times 10^{-4}$ for each case, with the data source indicated: ST, small wind tunnel; LT, large wind tunnel. (*b*) U/U_h at $x'/h = 1.42$ and $0.01h$ above the surface, as a function of Re.

Given that the mean pressure field is not significantly affected by Re one would expect the mean velocity field to be equally insensitive. This was demonstrated by making measurements of the axial velocity close to the top surface of the cube. In view of the very high turbulence intensities (and mean shear) there, HWA is inappropriate and the data was obtained using LDA (in both wind tunnels), PIV (in the small tunnel) and sonic anemometers in the field. Figure 7(*a*) shows a number of the resulting profiles. Note first that they clearly indicate that mean attachment occurs around $x'/h = 1.75$ – i.e. three-quarters of the distance along the top surface or actually just beyond that point, recognising that the profile was obtained at a distance $0.01h$ above the surface. Upstream of that location the mean flow is reversed. Second, the data obtained using PIV and (in the field) the sonic anemometers indicate noticeably more positive values of U/U_h. This is almost certainly a spatial resolution issue and is the major reason we include these PIV data. The acoustic path length of the sonic anemometers was equivalent to about $0.02h$, so these would be expected to overestimate U/U_h in this region of high shear. Similarly, a 16×16 pixel interrogation domain in analysing the PIV images implies a $1.25\,\text{mm} \times 1.25\,\text{mm}$ area – i.e. $0.016h \times 0.016h$, with equivalent doubling and halving of this for 32×32 or 8×8 pixel domains. It is clear that reducing the domain size led to noticeably lower U/U_h values, tending towards the LDA data (which were essentially genuine point measurements). The 16×16 data are quite close to those obtained with the sonic anemometer, so resolution effects are clearly similar in the two cases, reflecting the similarity in the normalized sampling volumes. Figure 7(*b*) shows the variation in U/U_h at $x'/h = 1.42$ with Re, using all the available data and, given these resolution effects for the PIV and sonic data, there is little sign of any significant Re sensitivity.

The data obtained for the 45° orientation of the cube lead in some respects to very different conclusions. Figure 8(*a*) shows the C_p distribution along the leading diagonal on the top surface and this data also seems insensitive to Re, as suggested by figure 8(*b*). There is a slight difference in the data from the two wind tunnels; this may be partly a result of slightly different tapping locations but is just as likely to be caused by the fact that such flows are inevitably slightly asymmetric; attachment onto the leading vertical edge at $y = 0$ is inherently unstable, so the flow tends to

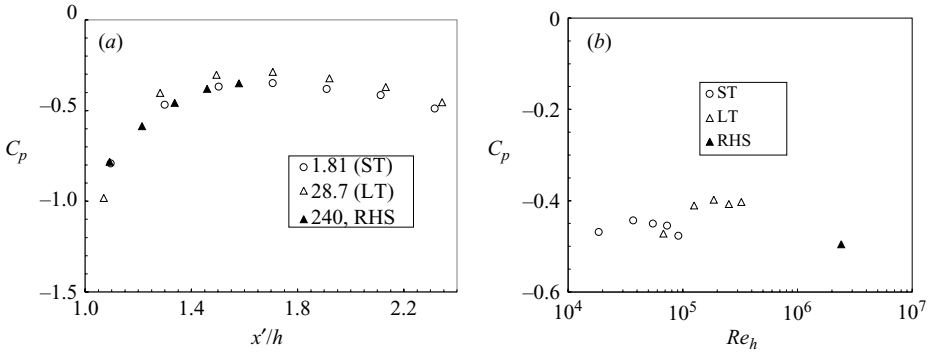

FIGURE 8. (*a*) The mean surface static pressure along the leading diagonal on the top surface of the cube at 45° to the approach flow. $x'/h = 1$ is the leading corner (so the trailing corner is at $x'/h = 2.414$). The legend gives the values of $Re \times 10^{-4}$ for each case, with the data source indicated: ST, small wind tunnel; LT, large wind tunnel. (*b*) The data at $x'/h = 1.215$ as a function of *Re*.

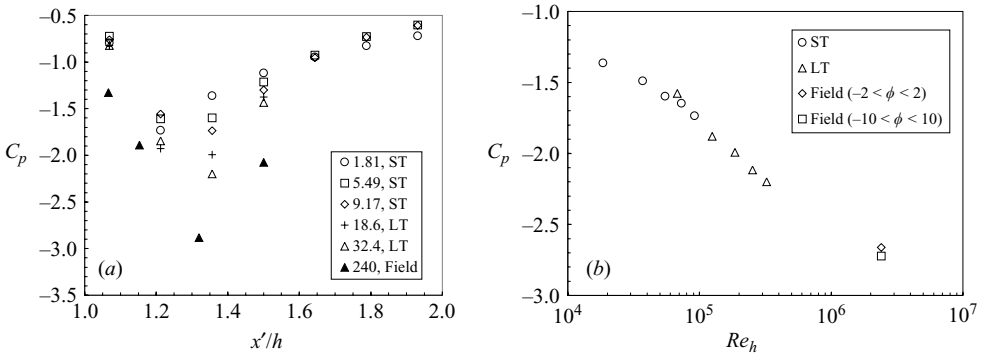

FIGURE 9. (*a*) The mean surface static pressure along a line parallel to the 45° leading edge and a distance $0.069h$ from it. The legend gives the values of $Re \times 10^{-4}$ for each case, with the data source indicated: ST, small wind tunnel; LT, large wind tunnel. (*b*) The data at $x'/h = 1.356$ as a function of *Re*.

prefer attachment at just one side or the other, depending on the fine details of the set-up. (See CR for discussion of this point). It is well known that in this 45° case, two delta-wing-type vortices are generated by the separation along the two top 45° leading edges. The effects of changes in the upstream turbulence characteristics are known to be much less significant for such cases. Indeed, even for a uniform laminar upstream flow CR showed that the pressure variation along the leading diagonal was very similar. So it is not surprising that the field data is in this case also similar (figure 8*a*). (Note that the 45° data is taken from Richards *et al.* (2001), since in their experiments the cube was physically rotated through 45° so that the upstream flow was unchanged; recall figure 5(*b*).) Despite the similarity between the wind-tunnel and field data, one might expect the flow immediately beneath the vortices to show some *Re* effects, because of the influence of changes in *Re* on the size and influence of the viscous core. Figure 9(*a*) shows the static-pressure variation along a line close and parallel to the 45° edge and, in complete contrast with all the earlier data, the profiles clearly depend strongly on *Re*. Note that in this case x' is measured in the 45° direction, starting with $x'/h = 1.0$ at the leading corner. Figure 9(*b*) shows C_p at

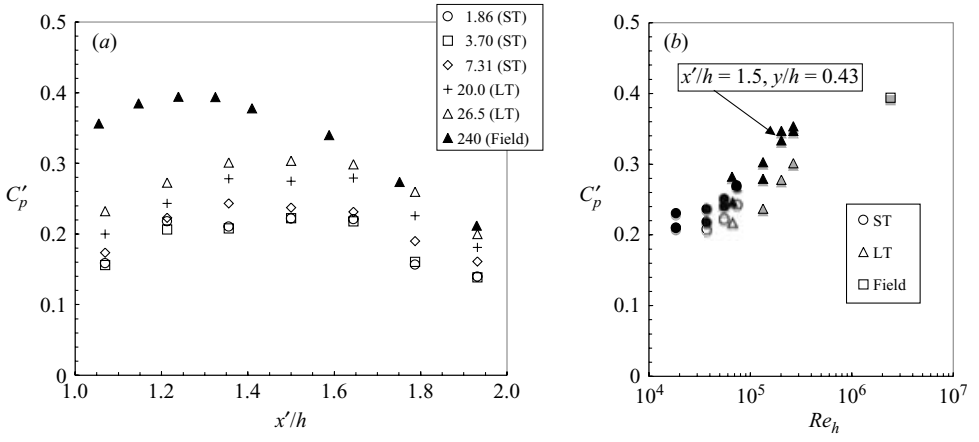

FIGURE 10. (*a*) The fluctuating surface static pressure along the axial centreline ($y = 0$) of the cube normal to the approach flow. (*b*) The data at $x'/h = 1.356$ as a function of *Re*. The solid symbols are for data at $x'/h = 1.5$, $y/h = \pm 0.43$.

the location $x'/h = 1.356$ and it clearly varies strongly and monotonically, becoming increasingly negative as *Re* increases. Even the field data point lies close to a linear extrapolation of the wind-tunnel data. Note also that the CR data (not shown), despite the very different upstream-turbulence characteristics, also agrees well with the present results.

It is difficult to avoid the general conclusion that, provided the bluff-body geometry and orientation is not such as to yield strong, relatively steady, vortical motions, *Re* effects on the mean pressure field are not significant; otherwise, however, and in certain regions of the flow, they are. C_p data collected at points near the top axial edges of the 0° cube do not show *Re* effects, so it is not justified to suppose that significant *Re* effects occur within regions near separation lines; only if the separation leads to unusually strong and concentrated vortex motions do such effects occur.

4.2. *Fluctuating data*

The fact that in some cases the mean flow, as characterized by surface pressures and near-surface velocities, is not significantly *Re*-dependent does not necessarily imply that the same independence would hold for fluctuating quantities like the r.m.s. pressure fluctuations or the mean square of the velocity fluctuations. Figure 10(*a*) shows C'_p profiles along the centreline top surface of the cube at 0°; C'_p is the r.m.s. value (corresponding in some cases to the mean C_p data shown in figure 6(*a*)). There clearly seems to be a Reynolds number effect, emphasized in figure 10(*b*), which shows C'_p at $x'/h = 1.36$ as a function of *Re*. It is interesting that the field data point again fits well with an extrapolation of the trend at lower *Re* even though the same is not true for the mean C_p value (see figure 6*b*). The *Re* dependency seen in figure 10(*a*) was also found in other profiles; measurements along the (top) transverse centreline (i.e. along $x'/h = 1.5$) were made, for example, and the results for two symmetrically placed points close to the two opposite edges (at $y/h = \pm 0.43$) are included in figure 10(*b*). The small differences between them at each *Re* are indicative of a slight asymmetry but the trend with *Re* seems clear and is the same as the trend found at points on the axial centreline.

In view of the differences in the levels of the upstream horizontal turbulence fluctuations between the tunnels and the field, one might ask whether the variation in

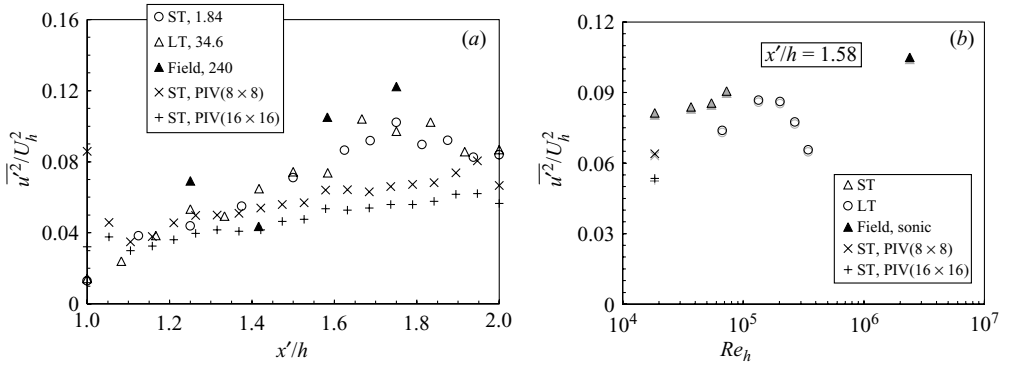

FIGURE 11. (*a*) The axial turbulence energy along the axial centreline of the cube ($y = 0$). (*b*) The data at $x'/h = 1.58$ as a function of *Re*.

C'_p seen in figure 10(*b*) is caused by variations in, say, u'/U_h at $z = h$ in the upstream flow. Quasi-steady theory (e.g. Richards & Hoxey 2004), in which fluctuations in surface loading are assumed to arise largely from the gustiness in the upstream flow, is sometimes used to estimate the variance and/or peak levels of the fluctuating pressure. For the normal cube orientation, where the variation in C_p with fluctuations in wind direction are relatively small, the theory suggests that a more appropriate normalization of p' would use $2u'U_h$, rather than U_h^2, where u' is the r.m.s. value of the velocity at $z = h$. However, replotting figure 10(*b*) as $C'_p/[2(u'/U_h)] \equiv p'/q'$ versus *Re*, where p' and q' refer to r.m.s. values of the surface pressure and the upstream dynamic pressure respectively, does not remove the *Re* trend. Plotting the same quantity against u'/U_h does not collapse the data either. Of course, quasi-steady theory is essentially a compromise and implicitly ignores the effects of unsteadiness and turbulence generated by the obstacle itself on the fluctuating surface pressures. One might not, therefore, expect to find such a collapse even in the absence of *Re* effects and, in any case, the normalization would clearly be inappropriate if the body were in a laminar flow (when $u' = 0$). It is emphasised that the trend seen in figure 10(*b*) is apparent within the wind-tunnel *Re* range, where the variations in u'/U_h with *Re* are, by design, insignificant (see figure 3). We conclude that although there must certainly be some effect of the different upstream characteristics between full-scale and laboratory situations, there remains a significant *Re* effect.

There is rather less evidence of *Re*-dependence in the fluctuating-velocity data. Figure 11, for example, shows the axial turbulence energy corresponding to the mean-velocity profiles near the surface given in figure 7. Given the (PIV) spatial-resolution issues discussed earlier, which lead to the underestimation of $\overline{u'^2}/U_h^2$, and the scatter in the data from the larger tunnel there is little evidence of any definitive trend with *Re*.

In contrast with the behaviour of C'_p for the normal-cube case (figure 10), the C'_p data along the axial diagonal for the case where the cube is at 45° to the approach flow were relatively insensitive to *Re*, as shown in figure 12. Only near the leading corner can a clear dependence on *Re* be seen and the trend is shown in figure 12(*b*), which includes data at $x'/h = 1.09$ (just downstream of the corner) and $x'/h = 1.707$ (the central point). Notice that in the central region of the top surface the fluctuations are significantly lower than they are when the cube is normal to the approach flow (cf. figure 10*a*), by at least a factor of 4. This is indicative of the dominance and relative steadiness of the central attached flow generated by the vortex pair

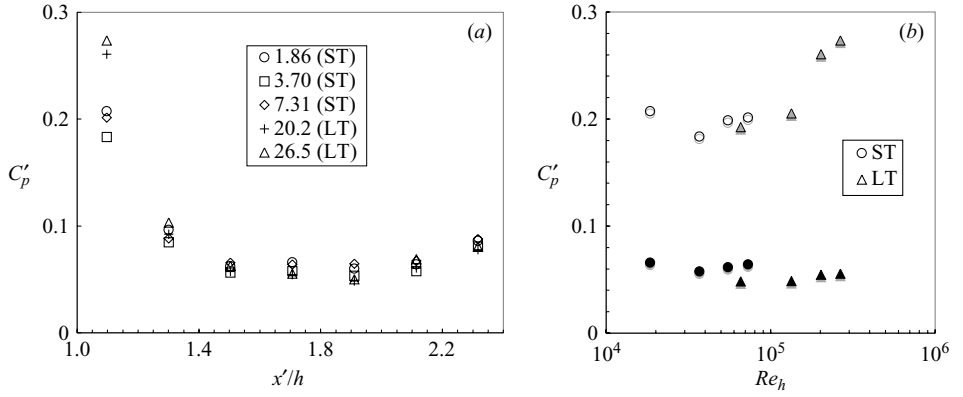

FIGURE 12. (*a*): fluctuating surface static pressure along top diagonal of cube at 45° to the approach flow ($y = 0$). (*b*): data at $x'/h = 1.09$ (open symbols) and 1.707 (the centre point, solid symbols) as a function of *Re*.

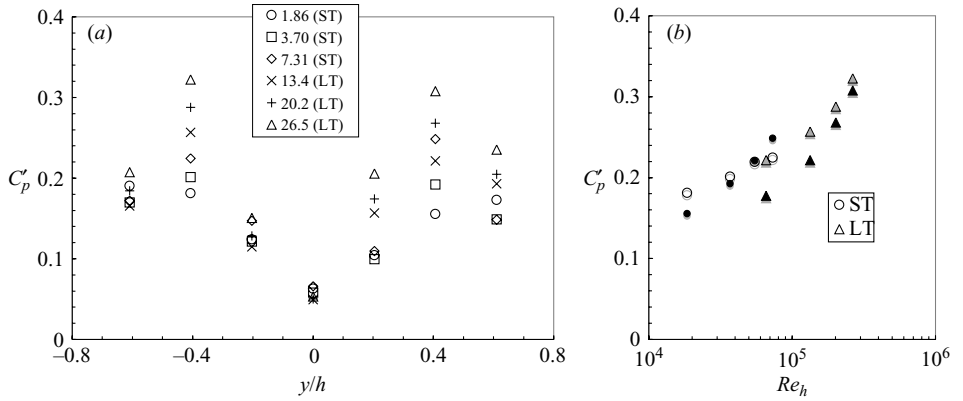

FIGURE 13. (*a*) The fluctuating surface static pressure along the transverse top diagonal of cube at 45° to the approach flow ($x'/h = 1.707$). (*b*) The data at $y/h = -0.41$ (open symbols) and $+0.41$ (solid symbols) as a function of *Re*.

created by separation from the $\pm 45°$ edges. However, these vortices themselves are not particularly steady, as shown by Kawai (2002) and, in addition and as argued earlier, are susceptible to *Re* changes. These two points are demonstrated by the data in figure 13, obtained along the transverse diagonal. Figure 13(*a*) shows the profiles of C_p' and it is clear that at positions roughly underneath the conical vortices (i.e. around $y/h = 0.4$) not only are the C_p' values very much higher than around the central region but they are also strongly dependent on *Re*. Figure 13(*b*), which shows data at $y/h = \pm 0.41$, emphasizes the latter point. Note again the slight asymmetry – rather greater for this 45° cube than for the normally oriented case, for reasons given earlier – but this does not mask the clear *Re* trend.

In those cases where no *Re* effect is evident, it is possible to suppose that a genuine *Re*-effect difference between field and laboratory is masked by an exactly counterbalancing effect of differences caused by large-scale motions in the field. But this seems highly unlikely; indeed, the data shown in figure 6(*b*), for example, might suggest quite the reverse, i.e. that there is no genuine *Re* effect (if there were it would be seen in the lower-*Re* wind-tunnel data) and it is the relatively larger energy

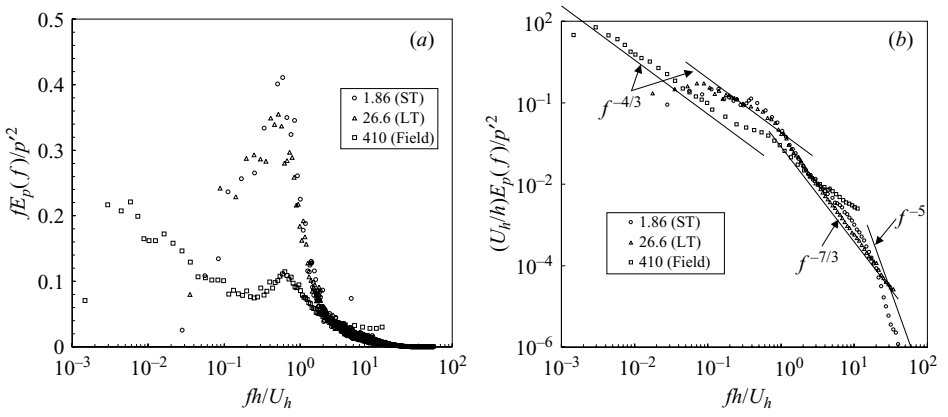

FIGURE 14. Surface pressure spectra measured near the central point, for the cube normal to the approach flow. (*a*): plotted so that the area is unity in each case; (*b*): plotted in the normal way, to emphasise behaviour in the high and medium frequency ranges. Note the straight solid and dashed lines, having the slopes indicated.

available at the largest scales in the field that leads to a rather more negative C_p near the leading edge of the body. Caution is needed here, however, in view of the limitations in the field data, discussed earlier. Notwithstanding this possible effect of the large-scale motions, there is little else in the data that could be taken as evidence that the relatively larger spread of scales in the field leads to significantly different flow behaviour around the body. Overall, the results discussed above indicate that nearly all the field data, whether for mean or fluctuating surface pressures or near-surface velocities, lie either on plausible extensions of the very clear *Re* trends in the wind-tunnel data or, in the absence of such trends, have mostly similar magnitudes to those measured in the laboratory.

The spectral content of the fluctuating-surface-pressure field is also worth some consideration. Detailed pressure spectra were not obtained for all surface locations and cube orientations but in figure 14 we show spectra obtained near the central point on the top of the cube normal to the approach flow. When plotted as $fE_p(f)$ versus fh/U_h, normalized so that the area under each plot is unity, as in figure 14(*a*), two features are immediately apparent. First, it is clear that in the field the relatively larger, lowest-frequency, motions in the upstream flow lead to a very much larger energy content in $C_{p'}$ at the largest scales. This is not, however, indicative of large differences in the character of the flow around the body although, as noted above, it is consistent with the discernibly lower C_p values in the field. Second, although plotting this way yields an inevitable peak in the spectrum, there is a separate secondary peak, discernible most clearly in the field data around $fh/U_h = 0.6$. This is more obvious for the laboratory data when using scaling expected to lead to spectral collapse in the high-frequency range, as shown in figure 14(*b*). In all cases, the small secondary hump occurs around $fh/U_h = 0.6$; it is masked in figure 14(*a*) in the laboratory data because it coincides roughly with the general peak. In the field data, the latter is at a much lower frequency (perhaps around $fh/U_h = 0.0025$ because of the relative dominance of the large-scale motions). This 'Strouhal' number, 0.6, is much higher than would be given by classical von Karman (alternate) vortex shedding, but it is similar to that typical for the in-phase shedding which has previously been noted in strongly three-dimensional flows around surface-mounted bodies. It is perhaps more likely, however,

that it reflects the time scale of the largest structures occurring in the separated shear layer above the body, as the attachment region is approached. A number of studies of two-dimensional separated flows have found that the peak spectral energies (in both velocity and surface pressure measured near reattachment) caused by these structures occur around $fx_R/U = 0.5$, where x_R is the distance between the reattachment and separation points (e.g. Hudy, Naguib & Humphreys 2003; Lee & Sung 2001). In the present case, for the cube normal to the flow, x_R is about $0.75h$ from the leading edge (see figure 7*a*), so $fx_R/U_h \approx 0.45$, suggesting a similar cause.

Further comments regarding figure 14(*b*) are appropriate. Whilst the sampling frequency for the lowest *Re* case was high enough to capture the expected (highest frequency) f^{-5} range before filtering or aliasing effects, the other two spectra do not extend that far but no doubt would have done if higher sampling rates had been used. (The pressure signal in the field, for example, was sampled at 25 Hz, yielding a normalized aliasing frequency near $fh/U_h = 12$, as evident in figure 14(*b*)). An inertial subrange might be expected to have a $f^{-7/3}$ slope and this is evident in the higher *Re* laboratory data and (marginally) at lower *Re*. In the field, however, the sampling rate was again too low to capture this region. At lower frequencies the field data have a substantial $f^{-4/3}$ region, as suggested by the 'superposition of vortices' model discussed by Hoxey, Quinn & Richards (2005). The laboratory data is not inconsistent with this slope, given the presence of the secondary hump. This $-4/3$ dependency is significantly different from the -1 slope normally expected of a regular boundary-layer pressure spectrum in the overlap region between the inertial range and the low-frequency parts of the spectrum (see e.g., Farabee & Casarella 1991; Goody 2004 and references therein). The flow above the top surface of the cube is of course very different from a regular boundary layer, and it appears that the combined vortex model of Hoxey *et al.* may have some merit.

5. Final remarks and conclusions

We conclude by emphasizing the major points arising from the work presented in this paper. First, for classes of bluff-body flow in which there are no strongly concentrated or relatively steady vortex regions, the mean pressure and velocity fields are not significantly *Re*-dependent. Our data extend well over two orders of magnitude in *Re*, from around 2×10^4 at the lowest. However, the fluctuating statistics may show a dependence on *Re*. This could well be caused simply by the slowly extending range of scales in the energy spectra as *Re* increases, measured by increasing λ/h values, even if the basic upstream flow properties (such as the mean shear, the turbulence levels and particularly Melbourne's parameter) remain essentially constant. The major implication of this conclusion is that if only mean wind loads are of interest, the classical approach of scaling up from wind-tunnel tests is perfectly acceptable, for such flow classes, whereas if fluctuating loads are expected, *Re* corrections should be considered. Of course, in either case, appropriate simulation of the upstream flow, particularly at the smaller scales represented by, say, Melbourne's parameter, is required.

Second, and in contrast, for cases where strong concentrated vortices exist essentially independently of the nature of the upstream flow (and usually, rather, as a direct result of the body geometry and orientation), clear *Re* effects do exist in the mean-flow field. Not surprisingly these are most evident in regions close to the cores of the vortices, where the effects of changing λ/h (and even viscous effects) are likely to be more significant. There is also *Re*-dependency in the fluctuating statistics, although at locations remote from the concentrated vortices this is weak, which is similar

perhaps to that found in the first flow class noted above. The *Re* trends are evident at laboratory scales and may continue all the way up the *Re* range to typical field values, although this latter statement cannot be proved from the present data; there is an inevitable gap in the *Re* range above the largest laboratory *Re* and below the field *Re* (see figure 9*b*, for example), so one cannot be sure whether the data might become independent of *Re* within that gap region. *Re* variations in field experiments are always limited to a factor of only 2 or 3, which, given the non-stationary nature of the wind field, is usually insufficient to detect trends of statistical significance. The implication here is that, for vortex-dominated flows, even mean wind loads are likely to be *Re*-dependent so that corrections are required if full-scale data are to be derived from wind-tunnel results. Precisely how to make such corrections is unclear and requires further work.

Although all the results presented here have been for cubes there is no reason to suppose that the conclusions would not remain valid for other sharp-edged body shapes; rectangular objects of a wide variety of heights and aspect ratios produce flows containing strong relatively steady concentrated vortices, or not, depending on their orientation. The long-standing belief in *Re* similarity in bluff-body flows, particularly when there is significant turbulence in the upstream flow (which might intuitively be expected to strengthen the hypothesis), seems therefore to be generally questionable. Its validity depends both on the kind of flow that occurs and on the particular quantities of interest. Consequently, the design of laboratory experiments intended to act as surrogates for typical field cases should be undertaken with caution.

The authors wish to thank the wind-tunnel technical staff in the School of Engineering Sciences for their consistently cheerful help. Likewise, the help of the technical staff at Silsoe Research Institute in the execution of the field experiments was crucial and is gratefully acknowledged. This work was done as part of a programme supported by the Engineering and Physical Sciences Research Council, under grant number GR/S12135/01.

REFERENCES

Castro, I. P. & Robins, A. G. 1977 The flow around a surface mounted cube in uniform and turbulent streams. *J. Fluid Mech.* **79**, 307–335.

Cherry, N. J., Hillier, R. & Latour, M. E. M. P. 1984 Unsteady measurements in a separating and reattaching flow. *J. Fluid Mech.* **144**, 13–46.

Cook, N. J. 1973 On simulating the lower third of the urban adiabatic boundary layer in a wind tunnel. *Atmos. Environ.* **7**, 691.

Cook, N. J. 1978 Wind tunnel simulation of the adiabatic atmospheric boundary layer by roughness, barrier and mixing device methods. *J. Wind Engng Ind. Aero.* **3**, 157–176.

Davenport, A. 1999 The Missing Links. Plenary paper in *Wind Engineering into the* 21*st Century* (ed. A. Larson & F. M. Livesey), pp. 91–204. Balkema.

Djilali, N. & Gartshore, I. S. 1991 Turbulent flow around a bluff rectangular plate. Part 1: experimental investigation. *Trans. ASME: J. Fluids Engng* **113**, 51–59.

ESDU 1985 Characteristics of atmospheric turbulence near the ground. Part II: single point data for strong winds (neutral atmosphere). *Engineering Sciences Data Unit*, Item 85020.

Farabee, T. M. & Casarella, M. J. 1991 Spectral features of wall pressure fluctuations beneath turbulent boundary layers. *Phys. Fluids* A **3**, 2410–2420.

Goody, M. 2004 Empirical spectral model of surface pressure fluctuations. *AIAA J.* **42**, 1788–1794.

Hart, D. P. 2000 Super-resolution PIV by recursive local correlation. *J. Visualisation* **3**, 187–194.

Hillier, R. & Cherry, N. J. 1981 The effects of free stream turbulence on separation bubbles. *J. Wind Engng Ind. Aero.* **8**, 49.

Hoxey, R. P., Reynolds, A. M., Richards, G. M., Robertson, A. P. & Short, J. L. 1998 Observations of Reynolds number sensitivity in the separated flow region on a bluff body. *J. Wind Engng Ind. Aero.* **73**, 231–249.

Hoxey, R. P., Quinn, A. D. & Richards, G. M. 2005 Variations in static pressure – application to wind engineering. Paper 315 in *4th European & African Conference on Wind Engineering*.

Hudy, L. M., Naguib, A. M. & Humphreys, W. M. 2003 Wall-pressure-array measurements beneath a separating/reattaching flow region. *Phys. Fluids* **15**, 706–717.

Hunt, J. C. R. & Fernholz, H. H. 1975 Wind-tunnel simulation of the atmospheric boundary layer: a report on Euromech 50. *J. Fluid Mech.* **70**, 543–559.

Kaimal, J. C., Wyngaard, Y., Izumi, O. R. & Cote, O. R. 1978 Spectral characteristics of surface layer turbulence. *Q. J. R. Met. Soc.* **98**, 563–598.

Kawai, H. 2002 Local peak pressure and conical vortex on a building. *J. Wind Engng Ind. Aero.* **90**, 251–263.

Lee, I. & Sung, H. J. 2001 Characteristics of wall pressure fluctuations in separated and reattaching flow over a backward-facing step: Part I. Time-mean statistics and cross-spectral analysis. *Expts. Fluids* **30**, 262–272.

Melbourne, W. H. 1980 Turbulence effects on maximum surface pressures: a mechanism and possibility of reduction. In *Wind Engineering* (ed. J. E. Cermak), pp. 541–551. Pergamon.

Murakami, S. & Mochida, A. 1988 3D numerical simulation of airflow around a cubic model by means of $k-\epsilon$ model. *J. Wind Engng Ind. Aero.* **31**, 283–303.

Perry, A. E., Lim, K. L. & Henbest, S. M. 1987 An experimental study of the turbulence structure in smooth and rough wall turbulent boundary layers. *J. Fluid Mech.* **177**, 437–466.

Pope S. B. 2000 *Turbulent Flows.* Cambridge University Press.

Richards, G. M. & Hoxey, R. P. 2004 Quasi-steady theory and point pressures on a cubic building. *J. Wind Engng Ind. Aero.* **92**, 1173–1190.

Richards, G. M., Hoxey, R. P. & Short, L. J. 2000 Spectral models for the neutral atmospheric surface layer. *J. Wind Engng Ind. Aero.* **87**, 167–185.

Richards, G. M., Hoxey, R. P. & Short, L. J. 2001 Wind pressures on a 6 m cube. *J. Wind Engng Ind. Aero.* **89**, 1553–1564.

Saathoff, P. J. & Melbourne, W. H. 1997 Effects of free-stream turbulence on surface pressure fluctuations in a separation bubble. *J. Fluid Mech.* **337**, 1–24.

Snyder, W. H. 1994 Some observations of the influence of stratification on diffusion in building wakes. In *Stably Stratified Flows: Flow and Dispersion over Topography* (ed. I. P. Castro & N. J. Rockliff) pp. 301–324. Oxford University Press.

Tieleman, H. W. 2003 Wind tunnel simulations of wind loading on low-rise structures: a review. *J. Wind Engng Ind. Aero.* **91**, 1626–1649.